Journal of Materials Chemistry A

High-Throughput Computational Discovery of 3,218 Ultralow Thermal Conductivity and Dynamically Stable Materials by Dual Machine Learning Models

Journal:	*Journal of Materials Chemistry A*
Manuscript ID	TA-ART-08-2023-004874.R1
Article Type:	Paper
Date Submitted by the Author:	09-Oct-2023
Complete List of Authors:	Ojih, Joshua; University of South Carolina Shen, Chen; TU Darmstadt, Rodriguez, Alejandro; University of South Carolina Onyekpe, Uche; Coventry University Zhang, Hongbin; Technical University of Darmstadt, Institute of Materials Science Choudhary, Kamal; National Institute of Standards and Technology, Hu, Ming; University of South Carolina, Mechanical Engineering

High-Throughput Computational Discovery of 3,218 Ultralow Thermal Conductivity and Dynamically Stable Materials by Dual Machine Learning Models

Joshua Ojih,[1] Chen Shen,[2] Alejandro Rodriguez,[1] Uche Onyekpe,[3] Hongbin Zhang,[2,*] Kamal Choudhary,[4] and Ming Hu[1,*]

[1]Department of Mechanical Engineering, University of South Carolina, SC 29208, USA

[2]Institute of Materials Science, Technical University of Darmstadt, Darmstadt 64287, Germany

[3]Centre for Computational Sciences and Mathematical Modelling, Coventry University, Priory Road, Coventry, CV1 5FB, UK

[4]Materials Science and Engineering Division, National Institute of Standards and Technology, Gaithersburg, MD 20899, USA

ABSTRACT

Materials with ultralow lattice thermal conductivity (LTC) continue to be of great interest for technologically important applications such as thermal insulators and thermoelectrics. We report an efficient workflow combining high-throughput density functional theory (DFT) computing and *two* different types of machine learning (ML) models for fast and accurately screening ultralow LTC from large-scale inorganic crystals. Firstly, we train seven *classification* ML models on 8,077 data obtained from high-throughput full DFT calculations to classify 50,574 structures into positive and negative dispersions, among which 22,899 structures are dynamically stable. Secondly, with 4,041 high quality LTC data, we train three graph neural network *prediction* models to predict LTC. The LTC ML models are verified on 359 randomly selected structures. Our ML model successfully predicted 90% of 359 structures to possess ultralow LTC (less than 1 W/mK). Additional 3,218 structures with ultralow LTC are also predicted and provided. With

* Authors to whom all correspondence should be addressed. E-Mail: hongbin.zhang@tu-darmstadt.de (H.Z.); hu@sc.edu (M.H.)

further analysis of the correlation between LTC and material features, we identify two excellent material descriptors, that can be evaluated with low computational cost for efficient screening of ultralow LTC: the large P_3 parameter which represents large number of three-phonon scattering channels and the large thermal mean squared displacement which reflects the soft phonon modes in the lattice usually resulting in strong phonon anharmonicity. Our workflow integrating dual ML models offers a new route to accelerate the discovery of novel dynamically stable materials with a high success rate for predicting effective lattice thermal conductivity.

Keywords: Lattice Thermal Conductivity; Graph Neural Network; Machine Learning; Materials Screening; High-Throughput First Principles Computing

INTRODUCTION

Lattice thermal conductivity (LTC) measures the ability of solid materials to conduct heat through atom vibrations and affects their thermal transport performance. Therefore, there is a strong impetus to identify materials with either extremely high or low LTC and to further develop thermal management solutions for various applications such as electronics cooling[1], building materials[2] and energy systems[3]. Theoretically, the most reliable and highly accurate method to predict LTC is the density functional theory (DFT) based anharmonic lattice dynamics (ALD) coupled with the phonon Peierls-Boltzmann transport equation (BTE)[4,5]. Despite its great success in the past decade[6–10], such a method is computationally expensive for the high-throughput computation of LTC for a large number of materials, because it requires calculations of the harmonic and anharmonic (at least the third-order) interatomic force constants which is time- and resource-costly. Alternatively, other empirical models to evaluate LTC have been applied, including the Debye-Callaway model[11,12], Slack model[13], but these methods are less accurate[14]. The classical molecular dynamics (MD) simulation[15–19] can also be used to study the thermal transport processes and to predict the LTC of materials, however, the accuracy of this approach relies significantly on that of the underlying interatomic potentials which are challenging to obtain for a large number of materials[20,21], even with the help of the recently developed machine learning (ML) interatomic potential techniques[22,23].

ML has been successfully applied for solving complex problems and improving decision making at both the academic and industrial levels. For instance, multi-fidelity ML models offer the possibility of bridging the gap between accurate DFT-level and rough classical-level (such as MD and empirical models) results[24,25]. With given data, ML algorithms can determine the underlying associations, even if the relationship is highly nonlinear[26]. This allows reducing the number of DFT calculations needed to discover new materials, because ML models are based on statistical prediction and hence they are computationally less expensive[27,28]. On the other hand, ML has also

been used for the prediction of a vast spectrum of physical properties[29], such as mechanical properties of metal alloys[30,31] and formation energies of crystals[32–34]. Carrete et al.[35] and Liu et al.[36] have used ML to predict the LTC of half-Heusler structures by training on DFT LTC data. Pal et al[37]. combined the crystal graph convolutional neural network ML approach with DFT calculations to firstly evaluate the stability of quaternary chalcogenides and then to evaluate their thermal conductivities. Seko et al[38]. applied the Bayesian optimization approach based on a surrogate model trained on the calculated thermal conductivity of 101 structures with simple crystal structures and screened for 221 materials with low LTC based on only two descriptors. ML, in particular multilayer neural network, has been successfully used to build accurate interatomic potentials for MD simulations for thermal transport of certain materials as well[22,23]. An interesting question is whether more systematic ML with robust descriptors can be applied to model the LTC of materials spanning a vast chemical (i.e., composition and crystal structure) space.

In this work, we present a screening and prediction strategy for identifying materials with low LTC by investigating seven ML algorithms, including two graph neural network (GNN) for classification, and three additional GNN models for regression. The first step helps to classify 50,574 structures with no imaginary phonon modes and to eliminate the dynamically unstable structures. In the second step for the so-obtained 22,899 stable structures, we construct three GNN models trained directly on the crystal structures, as opposed to custom physical descriptors which helps improve the accuracy of the GNN model. Thorough screening of the 22,899 stable structures gives rise to reliable prediction of their LTCs, among which the LTC of 359 structures are verified with explicit DFT calculations with an accuracy of 90% that have ultralow LTC. This paves the way to design thermal management materials for future applications. Analysis of the correlations between LTC and atomic and structural features reveals profound insights into the underlying mechanisms. We further propose the P_3 parameter and thermal mean square

displacements as an excellent material descriptor for quick screening crystalline materials with ultralow LTC.

Computational Methodology

Our approach comprises two major steps: (1) using an ML classifier to filter out unstable structures from a predefined pool of structures acquired from OQMD, and (2) training a regression model to recommend ultra-low LTC structures out of the stable structures identified in the first step. The entire workflow is shown in Figure S1 in the Supporting Information.

Data Acquisition from DFT: The optimal performance of the ML models requires high quality data either from high throughput calculations or from experiments. The initial structure pool to be screened contained 50,574 structures taken from OQMD and re-optimized by us using DFT with computational parameters described below. All structures have non-zero bandgaps, i.e., they are either semiconductors or insulators. For an effective screening of potentially dynamically stable structures, we first built a classification model using a dataset containing positive/negative frequency information of 8,077 structures calculated by DFT, among which 4,264 were dynamically stable structures (i.e., no imaginary frequencies in the phonon spectra were found along the high symmetry paths in the Brillouin zone), while the rest 3,813 were not dynamically stable (i.e., there are imaginary phonon modes). These 8,077 training data from OQMD contains seven crystal systems, with cubic crystal structures having the highest number. The dataset for all 8,077 structures used for classification model training with corresponding OQMD structure ID and the relevant material information is provided in the separate Excel file. Figure 1a, b shows the distribution of the crystal systems for our training and prediction data, where the distribution of the space group number for the cubic crystal structures is also shown. Figure 1c, d shows the element distribution in our training and predicted dataset. The entire dataset contains 63 elements in total across the periodic table. We did not explore the prediction of any crystal systems and elements outside of the training dataset. Once the classification model was trained, it was

then used to predict the 50,574 structure pool to screen the structures that are likely to be dynamically stable. After the classification model was deployed for screening, we finally obtained 22,899 stable structures.

For LTC ML model training, the data used were obtained from our DFT calculations on 4,041 crystal structures (3,317 cubic structures and 724 noncubic structures). Note that the total number of structures for DFT LTC dataset is slightly smaller than the above dynamically stable structures, because the BTE solutions for LTC were not converged for some structures. For the noncubic structures, since the LTC is anisotropic in general, the average LTC along the x, y, and z crystallographic direction was used in training our ML models. It is worth pointing out that all the ML models were trained on the log-scale LTC values, as our separate tests have proved significant performance improvement as compared to the models that were trained on the raw LTC values. The dataset for all 4,041 structures used for LTC ML model training with corresponding OQMD structure ID and the relevant material information is provided in the separate Excel file. All datasets used for classification and regression model training and LTC validation of crystal structures with OQMD structure ID, chemical formula, space group number, and other information are provided in the Excel file as supplemental data.

The DFT calculations were performed using the plane-wave basis projector augmented wave (PAW) method[39], within the Perdew-Burke-Ernzerhof exchange-correlation functional[40], as implemented in the Vienna ab initio simulation package (VASP)[41–43]. The cutoff energy was set to 520 eV for all crystal structures. The energy and force criteria for the DFT calculation of structure optimization were set to 10^{-8} eV and 10^{-4} eV/Å, respectively. The phonon band structures were determined using the frozen-phonon approach implemented in the PHONOPY package[44]. The second and third order interatomic force constant (IFCs) required for phonon band structure calculations were calculated using the compressive sensing lattice dynamics (CSLD) method[45], which extracts the IFCs from the Taylor-expanded interatomic forces in terms of atomic

displacements via the advanced compressive sensing technique. All atoms in supercells were randomly displaced with a magnitude of 0.03 Å by the PHONOPY package. The supercell size depends on the size of the primitive cell of each structure, but generally speaking the supercells with lattice parameter at least 10 Å for all 3 crystallographic directions were created. The CSLD method has the advantage of significantly lowering the number of supercells needed for IFCs fitting and hence the number of DFT calculations on supercells. For each supercell, 16 – 30 randomly displaced configurations were used for obtaining IFCs, depending on the symmetry of the materials. Generally, for noncubic structures a larger number of displaced supercells were generated. The energy and force criteria for the self-consistent DFT calculations of atomic forces in displaced supercells were set to 10^{-6} eV and 10^{-4} eV/Å, respectively. For k-points for electrons, we set up the product of the lattice parameter along each crystallographic direction and the corresponding number of k-points to be at least 40 Å. With IFCs obtained by DFT, the phonon dispersion calculations were done by the PHONOPY package, and the LTCs were obtained by solving the phonon Peierls-BTE with the ShengBTE package[4].

Data Analysis for ML Classification Training: The dataset consists of 8,077 unique data points with 7 attributes and one output value, i.e., yes or no for having or not having imaginary phonon frequencies, respectively. Figure 2 shows the relationship between each feature and the target. The somewhat monotonic relationship between the variables justifies the use of Spearman's rank correlation to evaluate the relationship between the features and the target for the classification problem. The Spearman correlation between the target column and input is shown in Figure 3. Most of the input attributes show a low negative correlation and low multicollinearity with the dependent variable. The number density, mass density, and bond length all have a positive correlation with the corresponding values being 0.15, 0.14, 0.04, respectively. Here, the bond length was calculated based on the geometry of the crystal structures. The neighbors within a cutoff radius of 6 Å of a central atom were considered to be bonded and we took the average of all bonding distance as the bond length of the central atom. This calculation

is repeated for every atom in the unit cell, and we finally take the average of all atoms as the final bond length of the structure. For the independent variable the highest positive and negative correlation values fall in a range of -0.25 to 0.15.

In checking the outliers in the data, an inter quartile range method was used, which is graphically visualized on a boxplot in Figure S2(a) in the Supporting Information. The observation contains an upper and lower boundary for which each of the attributes with observations outside the specified range is considered an outlier as described in Equations (1-3) and illustrated in Figure S2(b) in the Supporting Information.

$$\text{IQR} = Q3 - Q1 \quad (1)$$

$$\text{Upper Boundary} = Q3 + 1.5 \text{ Inter Quartile Range} \quad (2)$$

$$\text{Lower Boundary} = Q1 - 1.5 \text{ Inter Quartile Range} \quad (3)$$

Q3 is the 75th Quantile describing the upper half of the dataset and Q1 is the 25th Quantile describing the lower half of the dataset. We, however, found no performance benefit in removing the outliers from the data.

Machine Learning Model Training: For classification, seven ML models including two graph neural network models were trained in this study, namely, random forest (RF), extreme gradient boosting (XGBoost), logistic regression, CatBoost, Light GBM, atomistic line graph neural network (ALIGNN) and orbital graph convolution neural network (OGCNN). RF[46] is based on many decision trees and created by random feature selections and bagging[47] which helps to reduce overfitting by improving the accuracy and stability of the decisions trees, with performance demonstrated in image classification[48], fraud detection[49], etc. Boosting[50,51,52] is an ensemble method where series of decision trees are trained sequentially and each tree corrects the errors made by the previous tree. The XGBoost[53] is a scalable and efficient implementation of the gradient boosting technique[54,55], which creates new decision trees to fit the residuals of previous decision trees by minimizing the residual errors through a process of continuous iteration with

the aim of improving the prediction accuracy[56]. CatBoost[57,58,59] is based on the gradient boosting decision tree that is designed to handle categorical features in data. During the learning stage, decision trees are sequentially constructed to produce subsequent trees with decreased loss, and it uses ordered boosting to handle categorical features. The predictions from each tree are then combined to form the final prediction. Logistic regression[60] builds a logistic model for both classification and class probability estimation[61]. Light GBM[62] is a distributed high-performance framework that uses decision trees for ranking, classification, and regression tasks[63] with fast learning speed and high parallel efficiency for a large amount of data[64,65]. In contrast, for the regression three graph neural networks were used, namely, ALIGNN, OGCNN and global attention graph neural network (deeperGATGNN). For all ML models, data was split following the StratifiedKFold splitting strategy since the ML models were used to model a classification problem. Stratifying the split maintains the target class distribution in both the training and testing data. The ML objective is to maximize the accuracy of the binary classification models. The metric Accuracy and F1 scores were used to evaluate the performance of the binary classification models as the target class distribution is nearly balanced. For the regression models, the metric mean absolute error (MAE) was used to evaluate the performance of the models. All three graph neural networks, namely deeperGATNN[66], ALIGNN[67], and OGCNN[68], have found success in the material discovery for accurate and efficient prediction of material properties. They extract features from the crystal structures, which are then used for training the models. They combine the descriptors and learning models into one inseparable step. The model learns material properties directly from the connection of atoms in the crystal. For the effective application of the ML models for classification problem, a randomized search algorithm was used to find the optimal model hyperparameters. The ML models were trained on 75% of the training dataset and 25% was used for testing.

RESULT AND DISCUSSION

Results for classification models

Table 1 highlights the results describing the performance validation of the trained classification model for positive/negative dispersions on the 25% test data of the dataset. The ALIGNN model yields the highest performance among all classification models trained. It is worth pointing out that we added 4 more elemental descriptors[69] to the original 7 attributes for training, namely Pauling electronegativity, maximum principal quantum number, average number of electrons, and number of unpaired electrons. These descriptors are related to electron interaction, which we believe might improve our classification model. It turns out that the Pauling electronegativity has the highest feature importance. However, when we compared the accuracy of the new training with our previous training, there was only a slight improvement in the performance of the new model (results not shown here for brevity). More importantly, all traditional ML models with elemental descriptors did not outperform the graph neural model, i.e., the GNN model is still the best model with an accuracy of 0.861 and F1 score of 0.862 for ALIGNN. We therefore decided to use ALIGNN model to predict dynamic stability of the structures.

Figure 4 shows the confusion matrices for all 7 models to better visualize how the model classifies the stable and unstable structures. The confusion matrix shows the comparison between the predicted class label and the actual class label. For the ALIGNN model (the best performing model), we observe the 42.45% true positive, 7.63% false positive, 6.25% false negative and 43.55% true negative predictions. Thus, the model classifies the stable and unstable structures with high accuracy. Since the ALIGNN model exhibits the highest performance among all 7 classification models trained here, the ALIGNN was then used to predict the dynamic stability of the original pool of 50,574 structures, among which 22,899 structures were predicted as stable. This method helps us eliminate unstable structures from the original pool of data, and thereby accelerates the discovery of new materials with high accuracy and efficiency.

Results for regression models

For the LTC regression model, the ALIGNN is the best model among all three GNN models investigated, as evidenced by the relatively low MAE value as shown in Figure 5. This justifies the use of ALIGNN for further screening 22,899 stable structures to search for possible low LTC materials. From Figure 5 we can observe the performance of our models on the testing data. The ALIGNN model has an R^2 of 0.834 and MAE of 0.081 based on log-scale values, which means the model makes prediction that are within 0.081 of the log value of the actual LTC. The MAE based on the actual values are 6.986, 7.125, and 9.253 W/mK for the ALIGNN, OGCNN, and deeperGATGNN model, respectively. In Ref. [21] which uses crystal graph convolutional neural network (CGCNN) and RF ML models to train LTC, their models yield LTC prediction with MAE 0.14, R^2 0.85 and MAE 0.12, R^2 0.87, respectively. Compared to those models, our trained ALIGNN model has comparably good prediction performance and thus can be used for screening LTC in the future. The ALIGNN model performs very well because it incorporates bond angles information in the descriptors, which is an important factor contributing to phonon transport in crystalline materials in terms of both harmonic and anharmonic interatomic force constants. Similarly, the efficiency of ALIGNN model has also been demonstrated on training and prediction of phonon density of states[70], electronic density of states[71], superconducting properties[72], etc. It should be emphasized that, the performance of all ML models on LTC is slightly lower than that on other properties such as mechanical properties[25], heat capacity[28], sound speed, group velocity, etc. Although from domain knowledge the heat capacity is one of the dominant factors in obtaining LTC, it is easier to train because it is harmonic property (only depending on harmonic frequencies and temperature). It seems that the ML models in particular graph neural network models can easily capture the inherent relationship between atomic structure and harmonic vibrational frequencies. In contrast, LTC is a way more complex material property since it involves both harmonic and anharmonic nature of a lattice and most of time those effects are competing with each other. The only input to the LTC ML models is the atomic structure, where optimized

atomic positions and species are provided. However, those equilibrium positions do not contain enough information for the higher order interatomic interactions (the so-called phonon anharmonicity) in the crystalline structure, which plays a critical role in governing LTC. Thus, the ML models would likely underperform for LTC training and prediction.

All three models, namely ALIGNN, deeperGATGNN and OGCNN, were trained on the same dataset, and we compared the models based on the testing data using the MAE as metric of evaluation. We picked the best model for the prediction of our LTC. In GNN model training, the model learns descriptors directly from the crystal structures. The GNN models mainly use elements and atomic distance information as descriptors. They combine the descriptors and learning model into one inseparable step, i.e., the model learns material properties directly from the connection of atoms in the crystals[73]. The crystals structures are represented with a graph with nodes corresponding to atoms and edges corresponding to bonds. Still, there are some differences among the 3 GNN models. The ALIGNN model incorporates bond angles to the model. This new information helps to increase the accuracy of the model since many material properties are sensitive to slight change in bond angles. Bond angles can also be regarded as the representation of relative orientation between atoms' neighbors, which play a critical role in determining the anharmonicity of a material. Thus, it is understandable why the ALIGNN model has the highest performance in predicting LTC. The OGCNN model incorporates atomic orbital information to the descriptors. From chemistry point of view, atomic orbitals directly affect the interatomic interactions, thus the OGCNN model also has an excellent performance. The deeperGATGNN model can train a very deep network greater than 30 layers. However, since the total number of training data for our LTC by DFT calculations is only 4,014, which is far not large enough to maximize the advantage of very deep neural network. We anticipate that this is the most important reason why the deeperGATGNN model has the worst performance among the 3 GNN models. Overall, all 3 GNN models have additional features added or modified to the original construction, making them more accurate than traditional ML models.

Overall, we have trained a reliable ML model which we can use in screening and recommending potential low LTC structures. After predicting the LTC of the filtered 22,899 structures using the trained ALIGNN model, we randomly selected 359 materials with LTC predicted to be low (less than 10 W/mK) and validated their LTC by full DFT calculations. The calibration results of the ALIGNN model on these completely new structures are shown in Figure 6. It is observed that 321 of our 359 recommended structures have relatively low LTC values in the range of 0.1 – 10 W/mK at 300 K, corresponding to an accuracy of ~90% (321/359). In particular, 113 structures are verified to have LTC below 1 W/mK, i.e., ultralow LTC. Such a validation on the unseen structures results in an R^2 of 0.755 and MAE 0.265 and an absolute MAE of 9.08 W/mK. The two metrics are slightly off from those for model training and testing. This can be understood in terms of different data used. The training and test datasets contain majorly cubic structures, while the validation datasets are mostly non-cubic structures. In addition to the above 113 validated ultralow LTC structures, additional 3,218 structures are predicted to possess ultralow LTC. The predicted LTC of these untested structures, along with other relevant structural information, are provided in the Excel file as supplemental data.

We also noticed that our training data indeed has a lot of cubic structures, but the trained model learn from the atomic structures and also take into consideration the features of these structures, such as bond length, bond angles, etc. However, as we see from the validation of our 359 structures in Figure 6, they are completely new structures that have never been seen by the trained model. Specifically, 308 out 359 are noncubic structures, but the ALIGNN model still have very good performance in making predictions of their LTC. This can be understood in terms of the important or governing atomic features that might have been successfully captured or learned by the ALIGNN model, such as elements on the nodes, bond lengths (characteristic feature for the bonding strength which determines the group velocity of phonons), bond angles (the representation of relative orientation between atoms' neighbors or local environment, which

together with bond length determines the material symmetry and phonon anharmonicity of a material).

To validate the dynamic stability of our classification model, 359 structures were randomly selected. Here, we point out that, we actually take advantage of the DFT calculated LTC data to serve as calibration data for dynamic stability prediction, since any effective LTC data means the LTC BTE run is well converged and there must be no negative frequencies in the Brillouin zone, thus such data can be automatically used for validating dynamic stability prediction by our classification model. To this end, the dynamically stable structures were verified by the same 359 randomly selected structures, as done for validating regression model. We found all 359 structures have no negative frequencies in the Brillouin zone, and thus prove that the classification model has very high success rate for predicting true positive classification. Figure S3 in the Supporting Information shows the phonon dispersion of only four selected ultralow LTC materials out of our 359 structures recommended by our ALIGNN model. The phonon dispersion shows the relationship between the phonon frequency and wave vector in the Brillouin zone. All these materials which are predicted to be stable do not exhibit imaginary mode in the phonon spectra, which also validates our classification model. On the one hand, all structures have relatively low phonon frequencies (below 10 THz), in particular for low-lying acoustic phonon modes, which carry relatively low thermal energy with low group velocities and hence lead to low LTC. Optical phonons, on the other hand, exhibit island-like isolated dispersions, due to the considerable difference among the constitutive atom species. However, most optical phonon modes are flat band and thus have nearly zero group velocities and do not contribute much to thermal transport.

Physics insight into the structure-property relationship by ML models

In order to gain deep insight into the structure-property relationship, Figure 7 shows the t-distributed stochastic neighbor embedding (t-SNE)[74] plot for exploring and visualizing high

dimensional data in a 2D plot. The t-SNE plot provides a deep understanding of the correlation between LTC and atomic and structural properties. In Figure 7, the size of the circle denotes the magnitude of LTC, while the color bar indicates the atomic properties or the structural properties of the primitive cells. Figure 7a shows the correlation between mass density and LTC. We observe a positive correlation between mass density and LTC, which is consistent with domain knowledge and previous ML models[14]. Figure 7b shows the correlation between the total weight of structures and the LTC, where a negative correlation is found. This can be explained by two facts: (1) The phonon frequency is inversely proportional to the square root of the atomic mass and low phonon frequencies (heavy atoms) usually have relatively low group velocities. (2) Heavy atoms usually have stronger anharmonicity. According to the kinetic theory of phonons[75] these two effects lead to lower LTC for heavier atoms. Figure 7c shows that the number density (number of atoms per unit volume) is positively correlated with LTC, since the major effect of an increased number density is closer packed atomic structure and thus stronger interatomic bonding which favors thermal transport. Figure 7d shows the negative correlation between the number of atoms in the unit cell and LTC, because a larger number of atoms in the unit cell corresponds to a more complex atomic structure and leads to potentially enhanced phonon scattering and thus lower LTC. Figure 7e shows a correlation between bond length and LTC. The bond length refers to the average distance between the atomic nuclei in a repeating pattern of the crystal structures. It is also negatively correlated with LTC, because large bond length means the interatomic bonding is weak and more flexible, leading to stronger phonon anharmonicity and lower LTC. It should be noted that it is not straightforward to accurately correlate atomic properties of a single structure with its LTC. This can only be done when a large amount of data is available, and the features learned therein in a statistical way are more physically meaningful and the correlation identified is solider, while sometimes some outliers or out-of-trend could exist, since LTC is a very complex material property and it depends on many detailed factors like the crystal structures, compositions, bonding types, etc. Nevertheless, with high fidelity ML models for LTC, the t-SNE analysis

provides an intuitive understanding and observation of the underlying physics. It also generates a few descriptors for quick screening materials with target LTC (low or high) and training some ML LTC models with higher prediction performance.

Proposing new materials descriptors for fast and accurately screening ultralow LTC structures

Before closing, we explore the recommended materials by comparing the LTC and P_3 parameters. According to the domain knowledge and previous studies[76–78], the P_3 parameter represents three-phonon scattering phase space in the full Brillouin zone. A high P_3 parameter means a large number of phonon-phonon scattering channels in the crystals and thus generally corresponds to a low LTC. In this work, we found that the P_3 has a negatively large correlation value of -0.77 with LTC, which is consistent with phonon transport physics and previous studies. It is worth pointing out that it is expected to train the P_3 parameter much more easily by ML models with a very high accuracy than training on LTC. This is because the P_3 parameter is determined by scanning the possible combinations of three phonon frequencies that fulfill the physical conditions of three-phonon scattering process. Since all quantities involved in P_3 parameter calculation are phonon frequencies, which are the harmonic properties of the lattice, it is then natural to expect the ML models in particular the GNN models to easily capture this relationship. In fact, we continued to train the P_3 parameter by the ALIGNN, OGCNN, and DeeperGATGNN models on 4,041 DFT data (80% for training and 20% for testing) that was used for the same previous LTC regression models. The motivation behind this training is that we will verify from our 359 recommended structures whether the low LTC materials have high P_3 parameters and vice versa. Once confirmed, we can then recommend low LTC structures just by screening P_3 parameter or more importantly do an inverse design of hypothetical structures with the aid of P_3 parameter. Moreover, calculating P_3 parameters by full DFT only requires full quantification of harmonic phonon frequencies (second order IFCs) in the full Brillouin zone, and the computational cost is

significantly lower than calculating LTC which requires more computationally expensive third order IFCs.

In addition to the P_3 parameter, we further examine the thermal mean squared displacements (MSD) as related to the lattice thermal conductivity. Similar to the P_3 parameter, the MSD can be calculated for materials with phonon frequencies and corresponding eigenvectors from the second order IFCs, which also provide a low-cost descriptor for the LTC[44]. In essence, the MSD provides temperature-dependent displacements of atoms in the crystals, providing insight into atomic perturbations with respect to harmonic phonons. For instance, the high MSD is associated with weak bonding and/or low atomic density which is also tied with low sound velocity and LTC[79]. Additionally, rattling atoms may be discovered with unusually high MSD and has been proved to be responsible for strong phonon anharmonicity in insulating crystals[80]. We trained three GNN models, namely OGCNN, deeperGATGNN, and ALIGNN, for the MSD on the same 4,041 DFT data (80% for training and 20% for testing) that was used for the previous LTC regression and P_3 parameter models. Figure S4 and S5 shows the testing results for all three GNN models for P_3 parameter and MSDs. We can see that all three models have pretty good performance. Comparing Figures S4, S5, and Figure 5, we can observe that for the same training dataset, training on P_3 parameters has better overall performance than training on LTC, while training on MSD yields the worst performance. This confirms our previous hypothesis. As for MSD, the GNN models cannot be trained very well because the MSD is a complex property that relies on both phonon frequencies and corresponding eigenvectors, which is more complicated than P_3 parameter. We then used all three models to predict the P_3 parameter and MSD of the 22,899 dynamically stable structures. We finally validated the 359 recommended structures by comparing their P_3 parameters and MSD using LTC as the color map in Figure 8a (for DFT data) and Figure 8b (for predicted data). Figures 8a and 8b show the same color pattern distribution, being the red color (ultralow LTC) occurring in the top-right corner while the blue color (relatively high LTC) occurring in the bottom-left corner. This indicates that both P_3 parameter and MSD

have strong correlation with LTC, which is consistent with Figure S6. The same color pattern in Figures 8a and 8b also implies that the GGN models are well trained for both P_3 parameter and MSD, and the model predictions are accurate. More importantly, from Figure 8 we clearly see the trend that crystalline structures with high P_3 parameters and high MSDs have low LTC. These results evidently show that both P_3 parameter and MSD, which are relatively easier to calculate by full DFT and train by ML models with high precision, can serve as excellent material descriptors with low computational cost for quick screening materials with ultralow LTC, which provides a useful and indirect route for researchers to screen ultralow LTC by P_3 and MSD via either high-throughput DFT calculations or training ML models. As more reliable LTC data comes out in the near future, we anticipate that new and easier-to-calculate material descriptors or features will be identified by big data analysis.

Before closing, we would like to point out that, the main purpose of this work is to present a workflow of combining two different types of ML models for fast and accurately screening ultralow LTC from large-scale crystals, each corresponding to solve a critical problem in new thermal material discovery. Specifically, the classification model aims to filter out dynamically stable materials first, while the regression models aim to predict physically meaningful LTC values. Due to the large number of screened structures with low thermal conductivities (3,218), it is very time consuming to check all of them in the literature. Nevertheless, we believe our predicted ultralow LTC materials should have pretty high precision. For example, we find that several prototypes have already been proved by previous experiments with similar materials possessing ultralow LTC, including but not limited to full Heuslers (ABC_2 type with space group no. 225)[81], double perovskites ($ABCD_6$ type with space group no. 216)[82], half-Heuslers (ABC type with space group no. 216)[83], quaternary Heuslers (ABCD type with space group no. 216)[84], single perovskites (ABC_3 type with space group no. 221)[85], layered materials (such as space groups no. 194, 187, 160, AB_2C_4 type with space group no. 139)[86]. We expect that the screened materials will stimulate experimentalists to perform possible synthesis and validation.

CONCLUSIONS

In summary, we have trained 7 ML models including 2 state-of-the-art GNN models for classifying 50,574 structures into dynamically stable/unstable categories. We further trained 3 GNN models for searching ultralow LTC. Cross-comparison of the prediction performance and model accuracy was conducted among different predictive models. We finally chose the ALIGNN model to make LTC prediction on 22,899 stable structures due to its high predictive accuracy as featured by its low MAE values. 3,218 structures are predicted to have ultralow LTC (below 1 W/mK). Insight into the correlation between LTC and various atomic and structural properties were gained by means of the t-SNE plot. We verified 359 unseen structures recommended by the ALIGNN model with high precision DFT calculations, of which 113 structures possess ultralow LTC. We further trained separate GNN models for P_3 parameters and thermal mean squared displacements. We identified strong negative correlations between predicted P_3 parameters and MSDs and real LTC values calculated by DFT. This proves that one can recommend ultralow LTC materials simply from P_3 parameter and MSD, which is a more convenient approach for high-throughput DFT calculations with relatively lower computational cost than LTC itself and easier to train high performance ML models. Finally, we emphasize that, the combination of the classification and regression models coupled with high-throughput DFT calculations is promising for accelerating the efficient discovery of novel dynamically stable materials with target physical properties. Including dynamical stability into ML models will significantly increase the success rate of predicting materials with potential experimental synthesis.

Acknowledgements

This work was supported by the NSF (award number 2030128, 2110033, 2311202, 2320292), NASA SC Space Grant Consortium REAP Program (Award No.: 521383-RP-SC004), SC EPSCoR/IDeA Program under NSF OIA-1655740 (23-GC01) and ASPIRE grant from the Office of the Vice President for Research at the University of South Carolina (project 80005046).

Author contributions

M.H. conveyed the idea and designed and supervised the study. J.O. performed the ML training and testing. C.S. and A.R. performed DFT calculations. A.R. and U.O. filtered the structures and analyzed the ML results. J.O. prepared the draft of the manuscript. H.Z., C.P., K.C., and M.H. revised the manuscript. All the authors contributed to discussions and interpretation of results in the manuscript.

Competing interests

The Authors declare no Competing Financial or Non-Financial Interests.

Data availability

All datasets used for classification and regression model training (8,077 structures for classification and 4,041 structures for regression) and LTC validation (359 structures) with OQMD structure ID, chemical formula, space group number, and other information are provided in the separate Excel file named 'Datasets_pub.xlsx'. The additional 3,218 structures that are predicted to have ultralow LTC (below 1 W/mK) are provided in the separate Excel file named 'Ultralow_LTC_Predictions.xlsx'. The GNN packages used are available at the GitHub.

References

(1) Arik, M.; Becker, C. A.; Weaver, S. E.; Petroski, J. Thermal Management of LEDs: Package to System. *Third Int. Conf. Solid State Light.* **2004**, *5187* (January), 64. https://doi.org/10.1117/12.512731.

(2) Balaji, N. C.; Mani, M.; Reddy, B. V. V. Discerning Heat Transfer in Building Materials. *Energy Procedia* **2014**, *54*, 654–668. https://doi.org/10.1016/j.egypro.2014.07.307.

(3) Prashun, G.; Vladan, S.; Eric, S. T. Computationally Guided Discovery of Thermoelectric Materials. *Nat. Rev. Mater.* **2017**, *2*, 1–16. https://doi.org/10.1038/natrevmats.2017.53.

(4) Li, W.; Carrete, J.; Katcho, N. A.; Mingo, N. ShengBTE: A Solver of the Boltzmann Transport Equation for Phonons. *Comput. Phys. Commun.* **2014**, *185* (6), 1747–1758. https://doi.org/10.1016/j.cpc.2014.02.015.

(5) Broido, D. A.; Malorny, M.; Birner, G.; Mingo, N.; Stewart, D. A. Intrinsic Lattice Thermal Conductivity of Semiconductors from First Principles. *Appl. Phys. Lett.* **2007**, *91* (23), 19–22. https://doi.org/10.1063/1.2822891.

(6) Ouyang, T.; Hu, M. Thermal Transport and Thermoelectric Properties of Beta-Graphyne Nanostructures. *Nanotechnology* **2014**, *25* (24). https://doi.org/10.1088/0957-4484/25/24/245401.

(7) Tang, D. S.; Qin, G. Z.; Hu, M.; Cao, B. Y. Thermal Transport Properties of GaN with Biaxial Strain and Electron-Phonon Coupling. *J. Appl. Phys.* **2020**, *127* (3). https://doi.org/10.1063/1.5133105.

(8) Wang, H.; Qin, G.; Li, G.; Wang, Q.; Hu, M. Low Thermal Conductivity of Monolayer ZnO and Its Anomalous Temperature Dependence. *Phys. Chem. Chem. Phys.* **2017**, *19* (20), 12882–12889. https://doi.org/10.1039/c7cp00460e.

(9) Wang, H.; Qin, G.; Yang, J.; Qin, Z.; Yao, Y.; Wang, Q.; Hu, M. First-Principles Study of Electronic, Optical and Thermal Transport Properties of Group III-VI Monolayer MX (M = Ga, In; X = S, Se). *J. Appl. Phys.* **2019**, *125* (24). https://doi.org/10.1063/1.5094663.

(10) Qin, G.; Hu, M. Accelerating Evaluation of Converged Lattice Thermal Conductivity. *npj Comput. Mater.* **2018**, *4* (1). https://doi.org/10.1038/s41524-017-0058-3.

(11) Callaway, J. Model for Lattice Thermal Conductivity at Low Temperatures. *Phys. Rev.* **1959**, *113* (4), 1046–1051. https://doi.org/10.1103/PhysRev.113.1046.

(12) Morelli, D. T.; Heremans, J. P.; Slack, G. A. Estimation of the Isotope Effect on the Lattice Thermal Conductivity of Group IV and Group III-V Semiconductors. *Phys. Rev. B - Condens. Matter Mater. Phys.* **2002**, *66* (19), 1953041–1953049. https://doi.org/10.1103/PhysRevB.66.195304.

(13) Slack, G. A. Nonmetallic Crystals With High Thermal Conductivity. **1973**, *34*, 321–335.

(14) Qin, G.; Wei, Y.; Yu, L.; Xu, J.; Ojih, J.; Rodriguez, A. D.; Wang, H.; Qin, Z.; Hu, M. Predicting Lattice Thermal Conductivity from Fundamental Material Properties Using Machine Learning Techniques. *J. Mater. Chem. A* **2023**. https://doi.org/10.1039/D2TA08721A.

(15) Hu, M.; Poulikakos, D. Graphene Mediated Thermal Resistance Reduction at Strongly Coupled Interfaces. *Int. J. Heat Mass Transf.* **2013**, *62* (1), 205–213. https://doi.org/10.1016/j.ijheatmasstransfer.2013.02.045.

(16) Zhang, X.; Hu, M.; Tang, D. Thermal Rectification at Silicon/Horizontally Aligned Carbon Nanotube Interfaces. *J. Appl. Phys.* **2013**, *113* (19). https://doi.org/10.1063/1.4804071.

(17) Bao, H.; Shao, C.; Luo, S.; Hu, M. Enhancement of Interfacial Thermal Transport by Carbon Nanotube-Graphene Junction. *J. Appl. Phys.* **2014**, *115* (5).

https://doi.org/10.1063/1.4864221.

(18) Zhang, X.; Hu, M.; Poulikakos, D. A Low-Frequency Wave Motion Mechanism Enables Efficient Energy Transport in Carbon Nanotubes at High Heat Fluxes. *Nano Lett.* **2012**, *12* (7), 3410–3416. https://doi.org/10.1021/nl300261r.

(19) Ojih, J. Master Thesis. University of South Carolina. Searching Extreme Mechanical Properties Using Active Machine Learning and Density Functional Theory. **2021**.

(20) Luo, Y.; Li, M.; Yuan, H.; Liu, H. Predicting Lattice Thermal Conductivity via Machine Learning : A Mini Review. **2023**, 1–11. https://doi.org/10.1038/s41524-023-00964-2.

(21) Zhu, T.; He, R.; Gong, S.; Xie, T.; Gorai, P.; Nielsch, K.; Grossman, J. C. Charting Lattice Thermal Conductivity for Inorganic Crystals and Discovering Rare Earth Chalcogenides for Thermoelectrics. *Energy Environ. Sci.* **2021**, *14* (6), 3559–3566. https://doi.org/10.1039/d1ee00442e.

(22) Rodriguez, A.; Liu, Y.; Hu, M. Spatial Density Neural Network Force Fields with First-Principles Level Accuracy and Application to Thermal Transport. *Phys. Rev. B* **2020**, *102* (3), 35203. https://doi.org/10.1103/PhysRevB.102.035203.

(23) Rodriguez, A.; Lam, S.; Hu, M. Thermodynamic and Transport Properties of LiF and FLiBe Molten Salts with Deep Learning Potentials. *ACS Appl. Mater. Interfaces* **2021**, *13* (46), 55367–55379. https://doi.org/10.1021/acsami.1c17942.

(24) Schütt, K. T.; Glawe, H.; Brockherde, F.; Sanna, A.; Müller, K. R.; Gross, E. K. U. How to Represent Crystal Structures for Machine Learning: Towards Fast Prediction of Electronic Properties. *Phys. Rev. B - Condens. Matter Mater. Phys.* **2014**, *89* (20), 1–5. https://doi.org/10.1103/PhysRevB.89.205118.

(25) Ojih, J.; Al-fahdi, M.; Rodriguez, A. D.; Choudhary, K. Efficiently Searching Extreme

Mechanical Properties via Boundless Objective-Free Exploration and Minimal First-Principles Calculations. 1–12. https://doi.org/10.1038/s41524-022-00836-1.

(26) Butler, K. T.; Davies, D. W.; Cartwright, H.; Isayev, O.; Walsh, A. Machine Learning for Molecular and Materials Science. *Nature* **2018**, *559* (7715), 547–555. https://doi.org/10.1038/s41586-018-0337-2.

(27) Kauwe, S. K.; Graser, J.; Vazquez, A.; Sparks, T. D. Machine Learning Prediction of Heat Capacity for Solid Inorganics. *Integr. Mater. Manuf. Innov.* **2018**, *7* (2), 43–51. https://doi.org/10.1007/s40192-018-0108-9.

(28) Ojih, J.; Onyekpe, U.; Rodriguez, A.; Hu, J.; Peng, C.; Hu, M. Machine Learning Accelerated Discovery of Promising Thermal Energy Storage Materials with High Heat Capacity. **2022**. https://doi.org/10.1021/acsami.2c11350.

(29) Schmidt, J.; Marques, M. R. G.; Botti, S.; Marques, M. A. L. Recent Advances and Applications of Machine Learning in Solid-State Materials Science. *npj Comput. Mater.* **2019**, *5* (1). https://doi.org/10.1038/s41524-019-0221-0.

(30) Chatterjee, S.; Murugananth, M.; Bhadeshia, H. K. D. H. δ TRIP Steel. *Mater. Sci. Technol.* **2007**, *23* (7), 819–827. https://doi.org/10.1179/174328407X179746.

(31) Bhadeshia, H. K. D. H.; Dimitriu, R. C.; Forsik, S.; Pak, J. H.; Ryu, J. H. Performance of Neural Networks in Materials Science. *Mater. Sci. Technol.* **2009**, *25* (4), 504–510. https://doi.org/10.1179/174328408X311053.

(32) Ghiringhelli, L. M.; Vybiral, J.; Levchenko, S. V.; Draxl, C.; Scheffler, M. Big Data of Materials Science: Critical Role of the Descriptor. *Phys. Rev. Lett.* **2015**, *114* (10), 1–5. https://doi.org/10.1103/PhysRevLett.114.105503.

(33) Meredig, B.; Agrawal, A.; Kirklin, S.; Saal, J. E.; Doak, J. W.; Thompson, A.; Zhang, K.;

Choudhary, A.; Wolverton, C. Combinatorial Screening for New Materials in Unconstrained Composition Space with Machine Learning. *Phys. Rev. B - Condens. Matter Mater. Phys.* **2014**, *89* (9), 1–7. https://doi.org/10.1103/PhysRevB.89.094104.

(34) Curtarolo, S.; Morgan, D.; Persson, K.; Rodgers, J.; Ceder, G. Predicting Crystal Structures with Data Mining of Quantum Calculations. *Phys. Rev. Lett.* **2003**, *91* (13), 1–4. https://doi.org/10.1103/PhysRevLett.91.135503.

(35) Carrete, J.; Li, W.; Mingo, N.; Wang, S.; Curtarolo, S. Finding Unprecedentedly Low-Thermal-Conductivity Half-Heusler Semiconductors via High-Throughput Materials Modeling. *Phys. Rev. X* **2014**, *4* (1). https://doi.org/10.1103/PhysRevX.4.011019.

(36) Liu, J.; Han, S.; Cao, G.; Zhou, Z.; Sheng, C.; Liu, H. A High-Throughput Descriptor for Prediction of Lattice Thermal Conductivity of Half-Heusler Compounds. *J. Phys. D. Appl. Phys.* **2020**, *53* (31). https://doi.org/10.1088/1361-6463/ab898e.

(37) Pal, K.; Park, C. W.; Xia, Y.; Shen, J.; Wolverton, C. Scale-Invariant Machine-Learning Model Accelerates the Discovery of Quaternary Chalcogenides with Ultralow Lattice Thermal Conductivity. *npj Comput. Mater.* **2022**, *8* (1), 1–12. https://doi.org/10.1038/s41524-022-00732-8.

(38) Seko, A.; Hayashi, H.; Tsuda, K.; Chaput, L.; Tanaka, I. Prediction of Low-Thermal-Conductivity Compounds with First-Principles Anharmonic Lattice-Dynamics Calculations and Bayesian Optimization. **2015**, *205901* (November), 1–5. https://doi.org/10.1103/PhysRevLett.115.205901.

(39) Blöchl, P. E. Projector Augmented-Wave Method. *Phys. Rev. B* **1994**, *50* (24), 17953–17979. https://doi.org/10.1103/PhysRevB.50.17953.

(40) Perdew, J. P.; Burke, K.; Ernzerhof, M. Generalized Gradient Approximation Made Simple. *Phys. Rev. Lett.* **1996**, *77* (18), 3865–3868.

https://doi.org/10.1103/PhysRevLett.77.3865.

(41) Kresse, G.; Hafner, J. Ab Initio Molecular Dynamics for Liquid Metals. *Phys. Rev. B* **1993**, *47* (1), 558–561. https://doi.org/10.1103/PhysRevB.47.558.

(42) Joubert, D. From Ultrasoft Pseudopotentials to the Projector Augmented-Wave Method. *Phys. Rev. B - Condens. Matter Mater. Phys.* **1999**, *59* (3), 1758–1775. https://doi.org/10.1103/PhysRevB.59.1758.

(43) Vargas-Hernández, R. A. Bayesian Optimization for Calibrating and Selecting Hybrid-Density Functional Models. *J. Phys. Chem. A* **2020**, *124* (20), 4053–4061. https://doi.org/10.1021/acs.jpca.0c01375.

(44) Togo, A.; Tanaka, I. First Principles Phonon Calculations in Materials Science. *Scr. Mater.* **2015**, *108*, 1–5. https://doi.org/10.1016/j.scriptamat.2015.07.021.

(45) Zhou, F.; Nielson, W.; Xia, Y.; Ozoliņš, V. Compressive Sensing Lattice Dynamics. I. General Formalism. *Phys. Rev. B* **2019**, *100* (18), 1–15. https://doi.org/10.1103/physrevb.100.184308.

(46) Breiman, L. Random Forests. *Mach. Learn. 2001 451* **2001**, *45* (1), 5–32. https://doi.org/10.1023/A:1010933404324.

(47) Breiman, L. Bagging Predictors. *Mach. Learn. 1996 242* **1996**, *24* (2), 123–140. https://doi.org/10.1023/A:1018054314350.

(48) Bosch, A.; Zisserman, A.; Munoz, X. Image Classification Using Random Forests and Ferns. *Diangong Jishu Xuebao/Transactions China Electrotech. Soc.* **2007**, *22* (2), 28–33.

(49) Kumar, M. S.; Soundarya, V.; Kavitha, S.; Keerthika, E. S.; Aswini, E. Credit Card Fraud Detection Using Random Forest Algorithm. *2019 Proc. 3rd Int. Conf. Comput. Commun.*

Technol. ICCCT 2019 **2019**, 149–153. https://doi.org/10.1109/ICCCT2.2019.8824930.

(50) Schapire, R. E. A Brief Introduction to Boosting. **1999**.

(51) Opitz, D.; Maclin, R.; Bauer, E.; Chan, P.; Stolfo, S.; Wolpert, D.; Hussain, S.; Mustafa, M. W.; Jumani, T. A.; Baloch, S. K.; Alotaibi, H.; Khan, I.; Khan, A.; Zhang, Y.; Zhao, Z.; Zheng, J.; Prokhorenkova, L.; Gusev, G.; Vorobev, A.; Dorogush, A. V.; Gulin, A.; Nobre, J.; Neves, R. F.; Schapire, R. E.; Friedman, J. H.; Hastie, T.; Tibshirani, R.; Chen, T.; Guestrin, C.; Breiman, L.; Kalipe, G.; Gautham, V.; Behera, R. K.; Scikit Learn; Pedregosa F.; Varoquaux, G. . G. A. . M. V. . T. B. . G. O. . B. M. . P. P. . W. R. . D. V. . V. J. . P. A. . C. D. . B. M. . P. M. . D. E. Predicting Malarial Outbreak Using Machine Learning and Deep Learning Approach: A Review and Analysis. *Proc. - 2018 Int. Conf. Inf. Technol. ICIT 2018* **1999**, *24* (2), 6638–6648. https://doi.org/10.1016/J.EGYR.2021.07.008.

(52) Opitz, D.; Maclin, R. Popular Ensemble Methods: An Empirical Study. *J. Artif. Intell. Res.* **1999**, *11*, 169–198.

(53) Chen, T.; Guestrin, C. XGBoost: A Scalable Tree Boosting System. *Proc. 22nd ACM SIGKDD Int. Conf. Knowl. Discov. Data Min.* **2016**. https://doi.org/10.1145/2939672.

(54) Friedman, J.; Hastie, T.; Tibshirani, R. Additive Logistic Regression: A Statistical View of Boosting (With Discussion and a Rejoinder by the Authors). *https://doi.org/10.1214/aos/1016218223* **2000**, *28* (2), 337–407. https://doi.org/10.1214/AOS/1016218223.

(55) Friedman, J. H. Greedy Function Approximation: A Gradient Boosting Machine. *https://doi.org/10.1214/aos/1013203451* **2001**, *29* (5), 1189–1232. https://doi.org/10.1214/AOS/1013203451.

(56) Nobre, J.; Neves, R. F. Combining Principal Component Analysis, Discrete Wavelet Transform and XGBoost to Trade in the Financial Markets. *Expert Syst. Appl.* **2019**, *125*,

181–194. https://doi.org/10.1016/J.ESWA.2019.01.083.

(57) Hussain, S.; Mustafa, M. W.; Jumani, T. A.; Baloch, S. K.; Alotaibi, H.; Khan, I.; Khan, A. A Novel Feature Engineered-CatBoost-Based Supervised Machine Learning Framework for Electricity Theft Detection. *Energy Reports* **2021**, *7*, 4425–4436. https://doi.org/10.1016/J.EGYR.2021.07.008.

(58) Zhang, Y.; Zhao, Z.; Zheng, J. CatBoost: A New Approach for Estimating Daily Reference Crop Evapotranspiration in Arid and Semi-Arid Regions of Northern China. *J. Hydrol.* **2020**, *588*, 125087. https://doi.org/10.1016/J.JHYDROL.2020.125087.

(59) Prokhorenkova, L.; Gusev, G.; Vorobev, A.; Dorogush, A. V.; Gulin, A. CatBoost: Unbiased Boosting with Categorical Features. *Adv. Neural Inf. Process. Syst.* **2017**, *2018-Decem*, 6638–6648. https://doi.org/10.48550/arxiv.1706.09516.

(60) Cox, D. R. The Regression Analysis of Binary Sequences. *J. R. Stat. Soc. Ser. B* **1958**, *20* (2), 215–232. https://doi.org/10.1111/j.2517-6161.1958.tb00292.x.

(61) Aleksandra Bartosik, H. W. *Chapter 7 - Evaluating Safety and Toxicity*; Ashenden, S. K., Ed.; 2021. https://doi.org/doi.org/10.1016/B978-0-12-820045-2.00008-8.

(62) Ke, G.; Meng, Q.; Finley, T.; Wang, T.; Chen, W.; Ma, W.; Ye, Q.; Liu, T. Y. LightGBM: A Highly Efficient Gradient Boosting Decision Tree. *Adv. Neural Inf. Process. Syst.* **2017**, *2017-Decem* (Nips), 3147–3155.

(63) Gu, J. A Novel Credit Risk Assessment Model Based on LightGBM. **2020**, *8* (3), 71–73.

(64) Yang, S.; Zhang, H. Comparison of Several Data Mining Methods in Credit Card Default Prediction. *Intell. Inf. Manag.* **2018**, *10* (05), 115–122. https://doi.org/10.4236/iim.2018.105010.

(65) Zhou, Y.; Wang, W.; Wang, K.; Song, J. Application of LightGBM Algorithm in the Initial

Design of a Library in the Cold Area of China Based on Comprehensive Performance. *Buildings* **2022**, *12* (9). https://doi.org/10.3390/buildings12091309.

(66) Omee, S. S.; Louis, S.-Y.; Fu, N.; Wei, L.; Dey, S.; Dong, R.; Li, Q.; Hu, J. Scalable Deeper Graph Neural Networks for High-Performance Materials Property Prediction. *Patterns* **2021**, *3* (5), 100491. https://doi.org/10.1016/j.patter.2022.100491.

(67) Choudhary, K.; DeCost, B. Atomistic Line Graph Neural Network for Improved Materials Property Predictions. *npj Comput. Mater.* **2021**, *7* (1), 1–8. https://doi.org/10.1038/s41524-021-00650-1.

(68) Karamad, M.; Magar, R.; Shi, Y.; Siahrostami, S.; Gates, I. D.; Barati Farimani, A. Orbital Graph Convolutional Neural Network for Material Property Prediction. *Phys. Rev. Mater.* **2020**, *4* (9), 1–6. https://doi.org/10.1103/PhysRevMaterials.4.093801.

(69) Cai, X.; Zhang, Y.; Shi, Z.; Chen, Y.; Xia, Y.; Yu, A.; Xu, Y.; Xie, F.; Shao, H.; Zhu, H.; Fu, D.; Zhan, Y.; Zhang, H. Discovery of Lead-Free Perovskites for High-Performance Solar Cells via Machine Learning: Ultrabroadband Absorption, Low Radiative Combination, and Enhanced Thermal Conductivities. *Adv. Sci.* **2022**, *9* (4), 1–15. https://doi.org/10.1002/advs.202103648.

(70) Gurunathan, R.; Choudhary, K.; Tavazza, F. Rapid Prediction of Phonon Structure and Properties Using the Atomistic Line Graph Neural Network (ALIGNN). *Phys. Rev. Mater.* **2023**, *7* (2), 23803. https://doi.org/10.1103/PhysRevMaterials.7.023803.

(71) Kaundinya, P. R.; Choudhary, K.; Kalidindi, S. R. Prediction of the Electron Density of States for Crystalline Compounds with Atomistic Line Graph Neural Networks (ALIGNN). *Jom* **2022**, *74* (4), 1395–1405. https://doi.org/10.1007/s11837-022-05199-y.

(72) Choudhary, K.; Garrity, K. Designing High-TC Superconductors with BCS-Inspired Screening, Density Functional Theory, and Deep-Learning. *npj Comput. Mater.* **2022**, *8*

(1), 1–12. https://doi.org/10.1038/s41524-022-00933-1.

(73) Xie, T.; Grossman, J. C. Crystal Graph Convolutional Neural Networks for an Accurate and Interpretable Prediction of Material Properties. *Phys. Rev. Lett.* **2018**, *120* (14), 145301. https://doi.org/10.1103/PhysRevLett.120.145301.

(74) Hybridization, D.; Hardness, U. Diverse Hybridization and Ultrahigh Hardness. **2021**, 1–15.

(75) Wingert, M. C.; Chen, Z. C. Y.; Dechaumphai, E.; Moon, J.; Kim, J. H.; Xiang, J.; Chen, R. Thermal Conductivity of Ge and Ge-Si Core-Shell Nanowires in the Phonon Confinement Regime. *Nano Lett.* **2011**, *11* (12), 5507–5513. https://doi.org/10.1021/nl203356h.

(76) Elalfy, L.; Music, D.; Hu, M. Metavalent Bonding Induced Abnormal Phonon Transport in Diamondlike Structures: Beyond Conventional Theory. *Phys. Rev. B* **2021**, *103* (7), 1–18. https://doi.org/10.1103/PhysRevB.103.075203.

(77) Ouyang, T.; Hu, M. Competing Mechanism Driving Diverse Pressure Dependence of Thermal Conductivity of XTe (X=Hg, Cd, and Zn) Competing Mechanism Driving Diverse Pressure ... Tao Ouyang and Ming Hu. *Phys. Rev. B - Condens. Matter Mater. Phys.* **2015**, *92* (23), 1–13. https://doi.org/10.1103/PhysRevB.92.235204.

(78) Yue, S. Y.; Qin, G.; Zhang, X.; Sheng, X.; Su, G.; Hu, M. Thermal Transport in Novel Carbon Allotropes with Sp2 or Sp3 Hybridization: An Ab Initio Study. *Phys. Rev. B* **2017**, *95* (8), 1–11. https://doi.org/10.1103/PhysRevB.95.085207.

(79) Ju, S.; Yoshida, R.; Liu, C.; Wu, S.; Hongo, K.; Tadano, T.; Shiomi, J. Exploring Diamondlike Lattice Thermal Conductivity Crystals via Feature-Based Transfer Learning. *Phys. Rev. Mater.* **2021**, *5* (5), 1–2. https://doi.org/10.1103/PhysRevMaterials.5.053801.

(80) Jain, A.; Veeravenkata, H. P.; Godse, S.; Srivastava, Y. High-Throughput Computational

Discovery of 40 Ultralow Thermal Conductivity and 20 Highly Anisotropic Crystalline Materials. **2022**.

(81) He, J.; Amsler, M.; Xia, Y.; Naghavi, S. S.; Hegde, V. I.; Hao, S.; Goedecker, S.; Ozoliņš, V.; Wolverton, C. Ultralow Thermal Conductivity in Full Heusler Semiconductors. *Phys. Rev. Lett.* **2016**, *117* (4), 1–6. https://doi.org/10.1103/PhysRevLett.117.046602.

(82) Klarbring, J.; Hellman, O.; Abrikosov, I. A.; Simak, S. I. Anharmonicity and Ultralow Thermal Conductivity in Lead-Free Halide Double Perovskites. *Phys. Rev. Lett.* **2020**, *125* (4), 45701. https://doi.org/10.1103/PhysRevLett.125.045701.

(83) Zhang, X.; Huang, M.; Li, H.; Chen, J.; Xu, P.; Xu, B.; Wang, Y.; Tang, G.; Yang, S. Ultralow Lattice Thermal Conductivity and Improved Thermoelectric Performance in a Hf-Free Half-Heusler Compound Modulated by Entropy Engineering. *J. Mater. Chem. A* **2023**, *11* (15), 8150–8161. https://doi.org/10.1039/d3ta00631j.

(84) Rodriguez, A.; Lin, C.; Yang, H.; Al-Fahdi, M.; Shen, C.; Choudhary, K.; Zhao, Y.; Hu, J.; Cao, B.; Zhang, H.; Hu, M. Million-Scale Data Integrated Deep Neural Network for Phonon Properties of Heuslers Spanning the Periodic Table. *npj Comput. Mater.* **2023**, *9* (1). https://doi.org/10.1038/s41524-023-00974-0.

(85) Osei-Agyemang, E.; Adu, C. E.; Balasubramanian, G. Ultralow Lattice Thermal Conductivity of Chalcogenide Perovskite CaZrSe3 Contributes to High Thermoelectric Figure of Merit. *npj Comput. Mater.* **2019**, *5* (1). https://doi.org/10.1038/s41524-019-0253-5.

(86) Zhang, L. C.; Qin, G.; Fang, W. Z.; Cui, H. J.; Zheng, Q. R.; Yan, Q. B.; Su, G. Tinselenidene: A Two-Dimensional Auxetic Material with Ultralow Lattice Thermal Conductivity and Ultrahigh Hole Mobility. *Sci. Rep.* **2016**, *6* (October 2015), 1–9. https://doi.org/10.1038/srep19830.

Table 1. Performance evaluation of machine learning classification models for positive/negative phonon dispersions.

Algorithm	Accuracy	F1 Score
Light GBM	0.757	0.756
XGBoost	0.751	0.752
CatBoost	0.750	0.763
Random Forest	0.748	0.748
Logistic Regression	0.633	0.633
ALIGNN	0.861	0.862
OGCNN	0.846	0.854

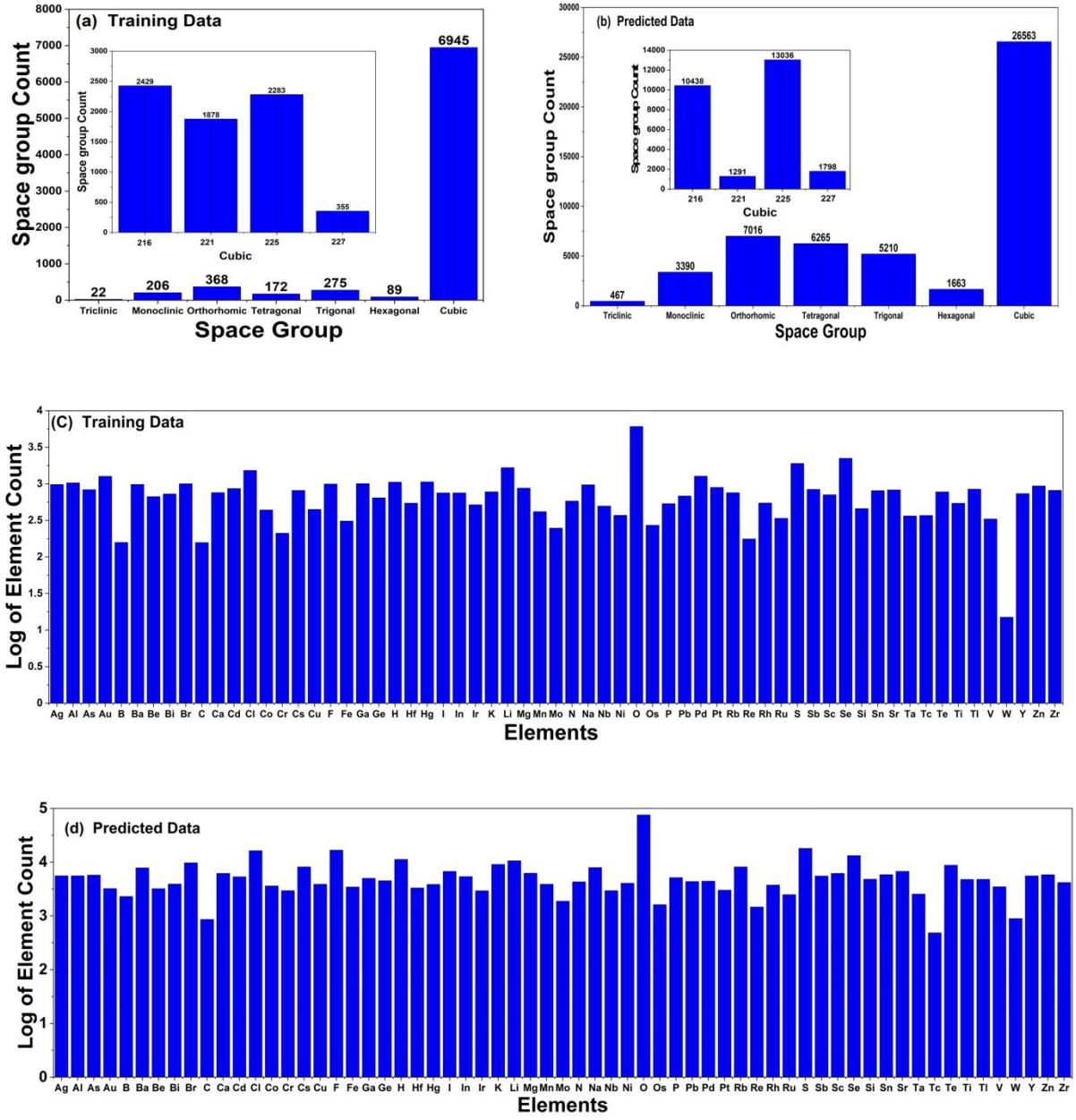

Figure 1: Distribution of symmetry of materials used for ML model (a) training and (b) prediction. The insets show the space group distribution of cubic structures. Distribution of elements in the structures used for ML model (c) training and (d) prediction, where logarithmic scale is used for the number of element count in y-axis.

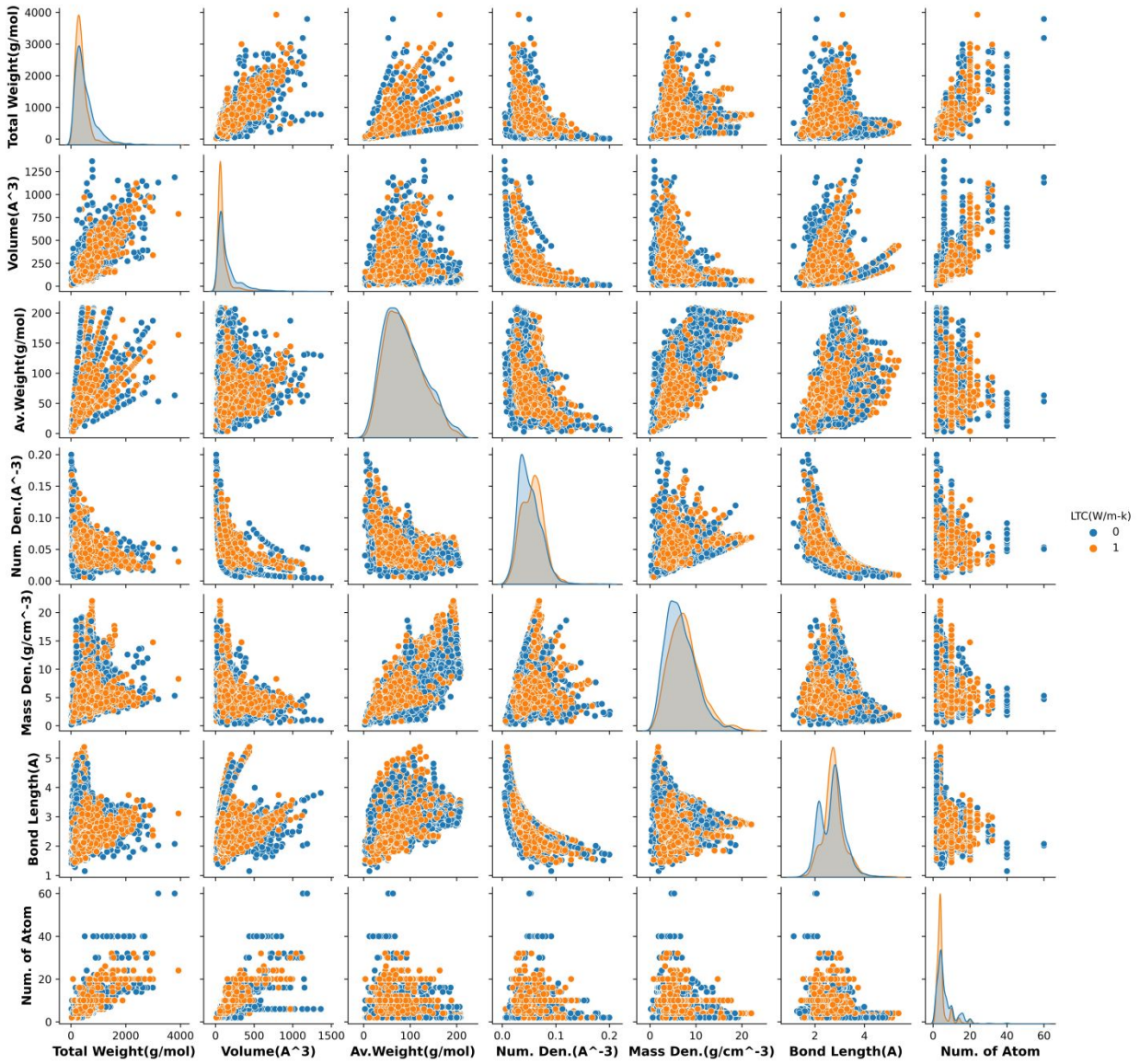

Figure 2: Scatter plot between attributes. This justifies the use of Spearman's rank correlation in evaluating the relationship between the attributes and target.

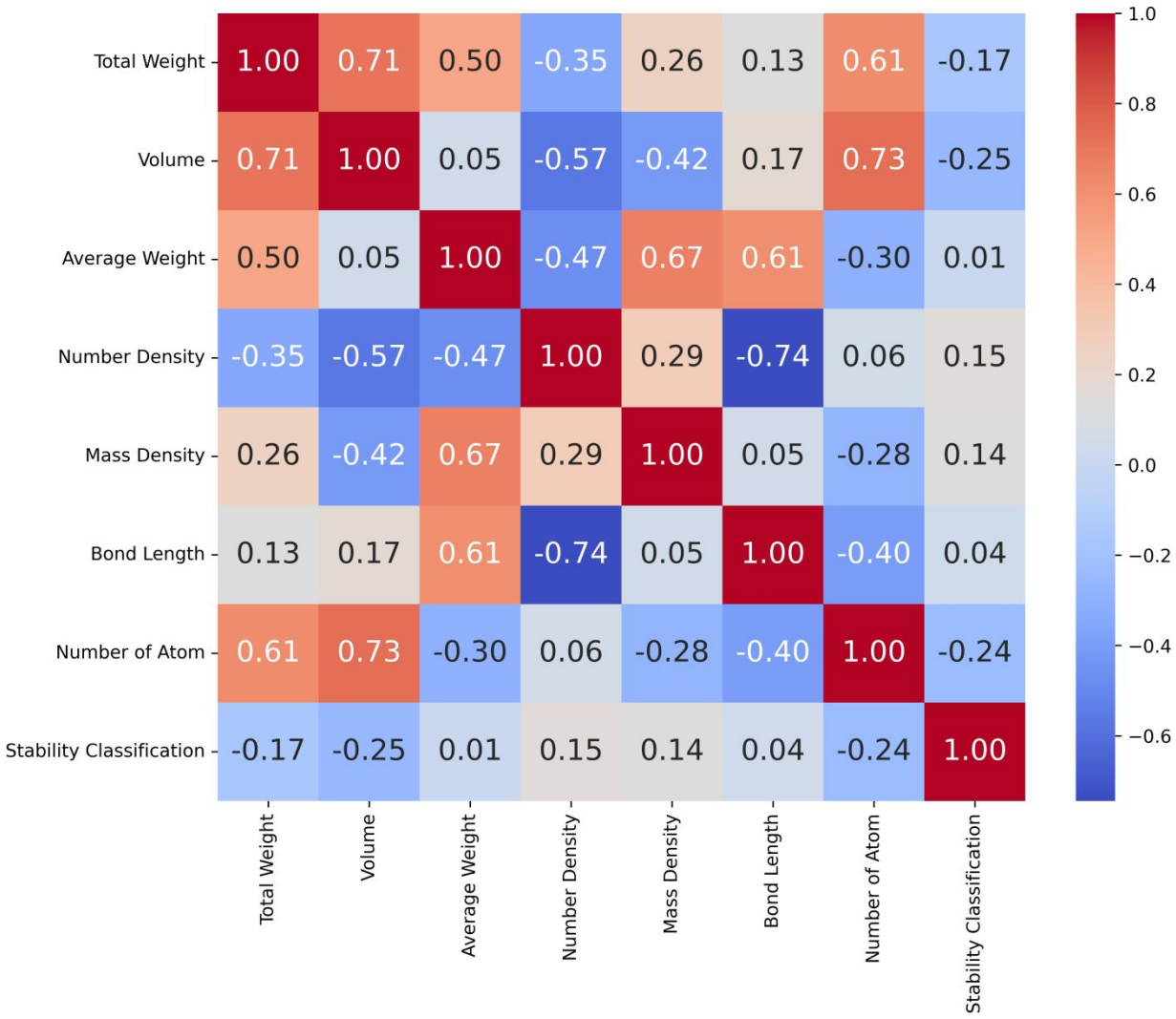

Figure 3: Spearman's rank multicollinearity study between the independent variables and the dependent variable for the classification model.

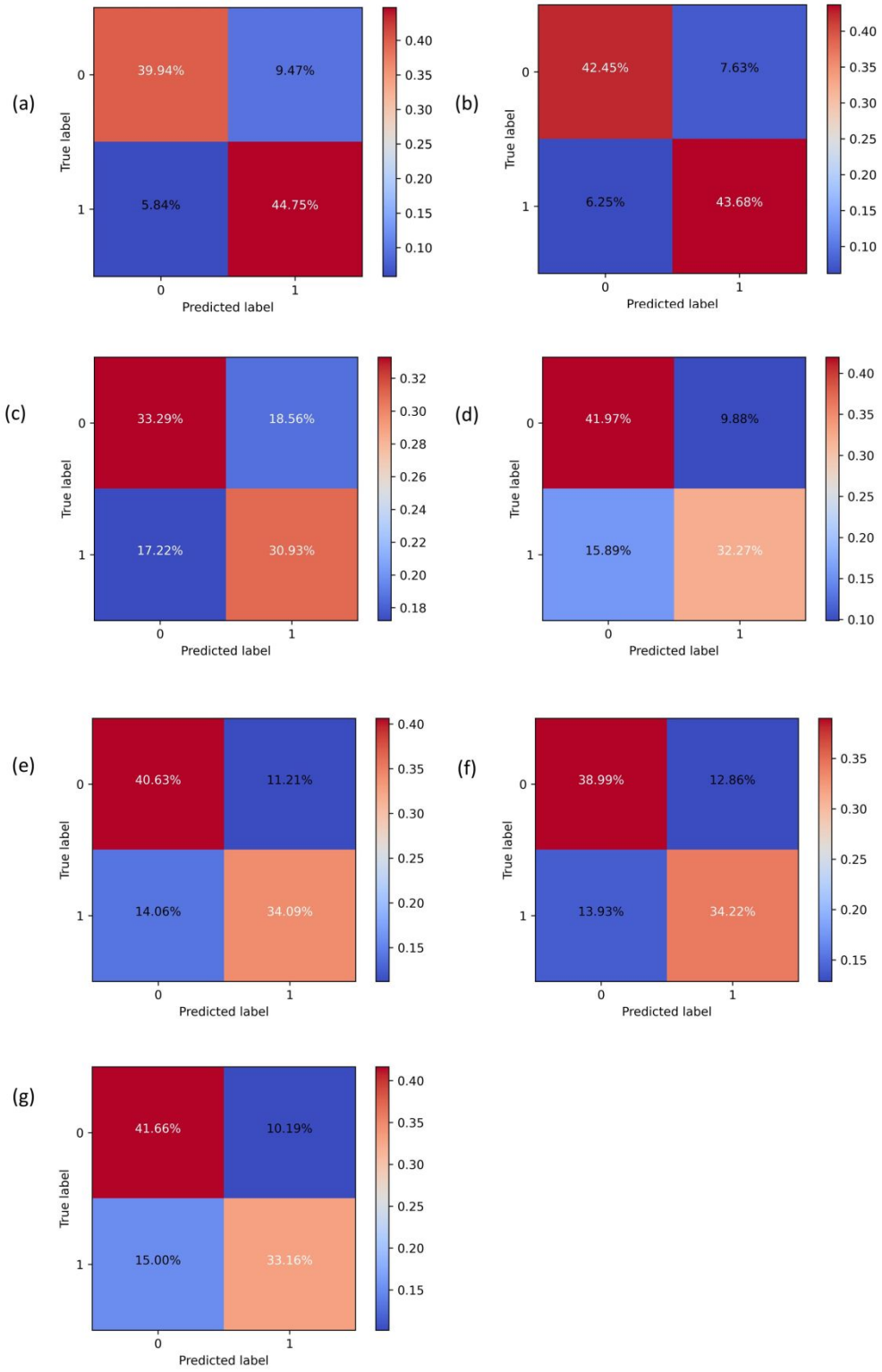

Figure 4: Confusion matrix heatmap (model performance metrics) for the trained ML and GNN models. (a) OGCNN, (b) ALIGNN, (c) Logistic regression, (d) Random Forest, (e) Light GBM, (f) XGBoost, and (g) CatBoost.

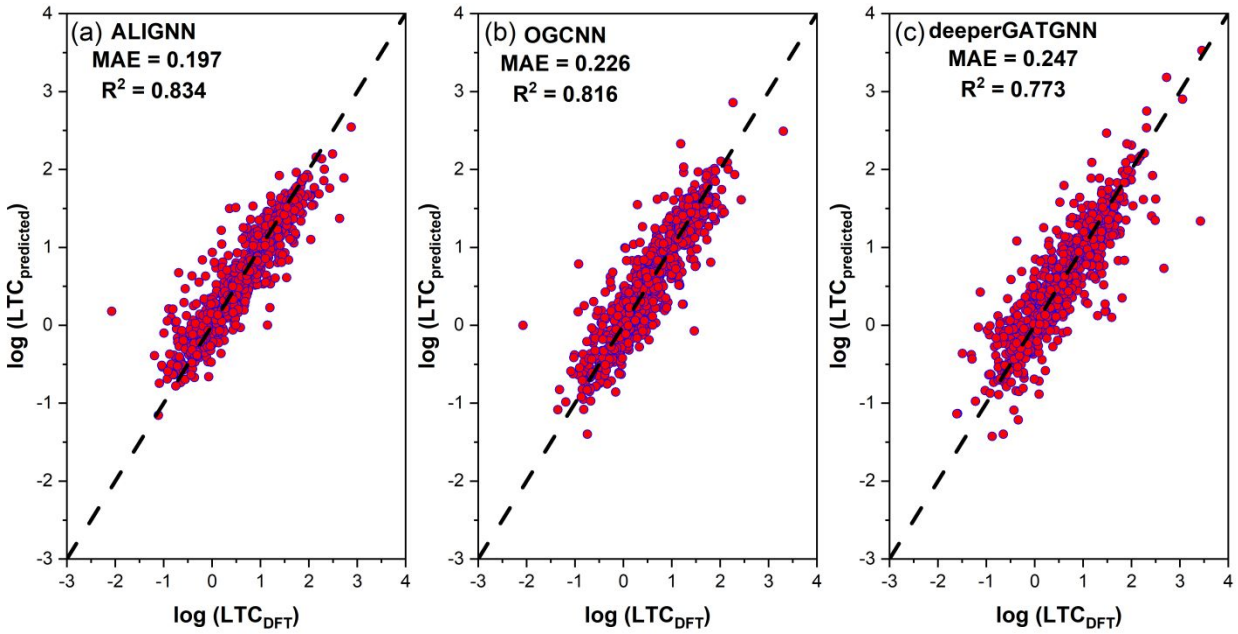

Figure 5: Testing results of lattice thermal conductivity (LTC) for the 3 graph neural network (GNN) models trained for 808 structures.

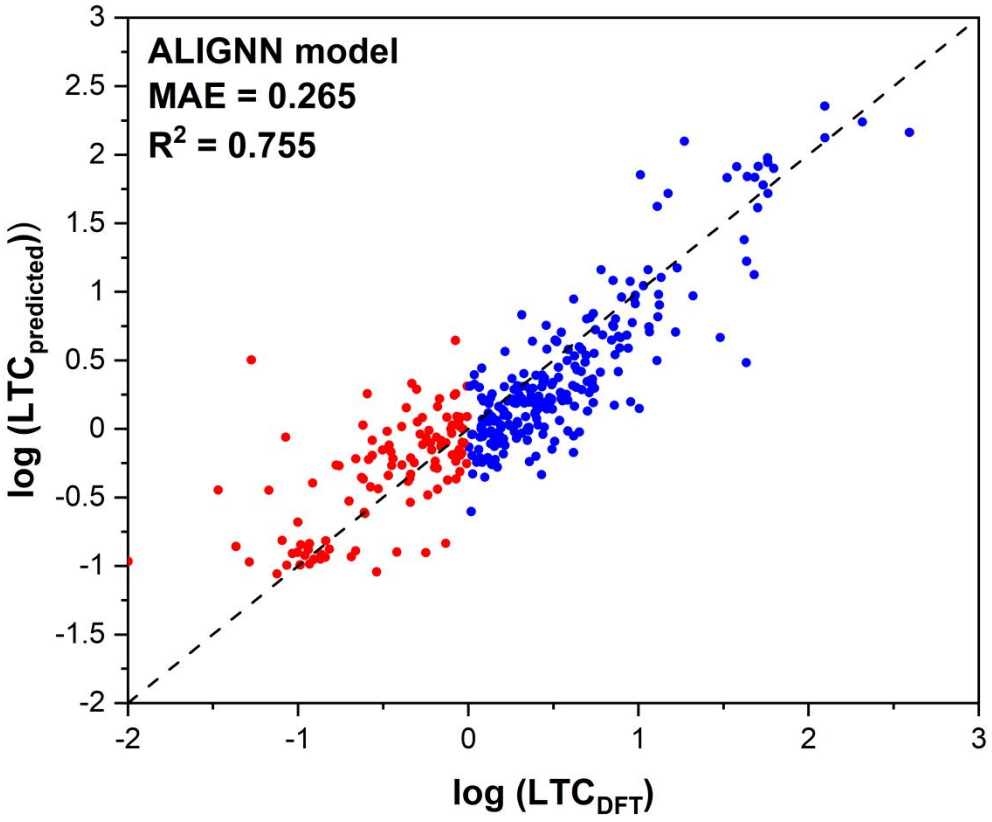

Figure 6: Validation of ALIGNN prediction for the 359 selected structures by full DFT calculations. The red color represents 113 structures with ultralow lattice thermal conductivity (less than 1 W/mK).

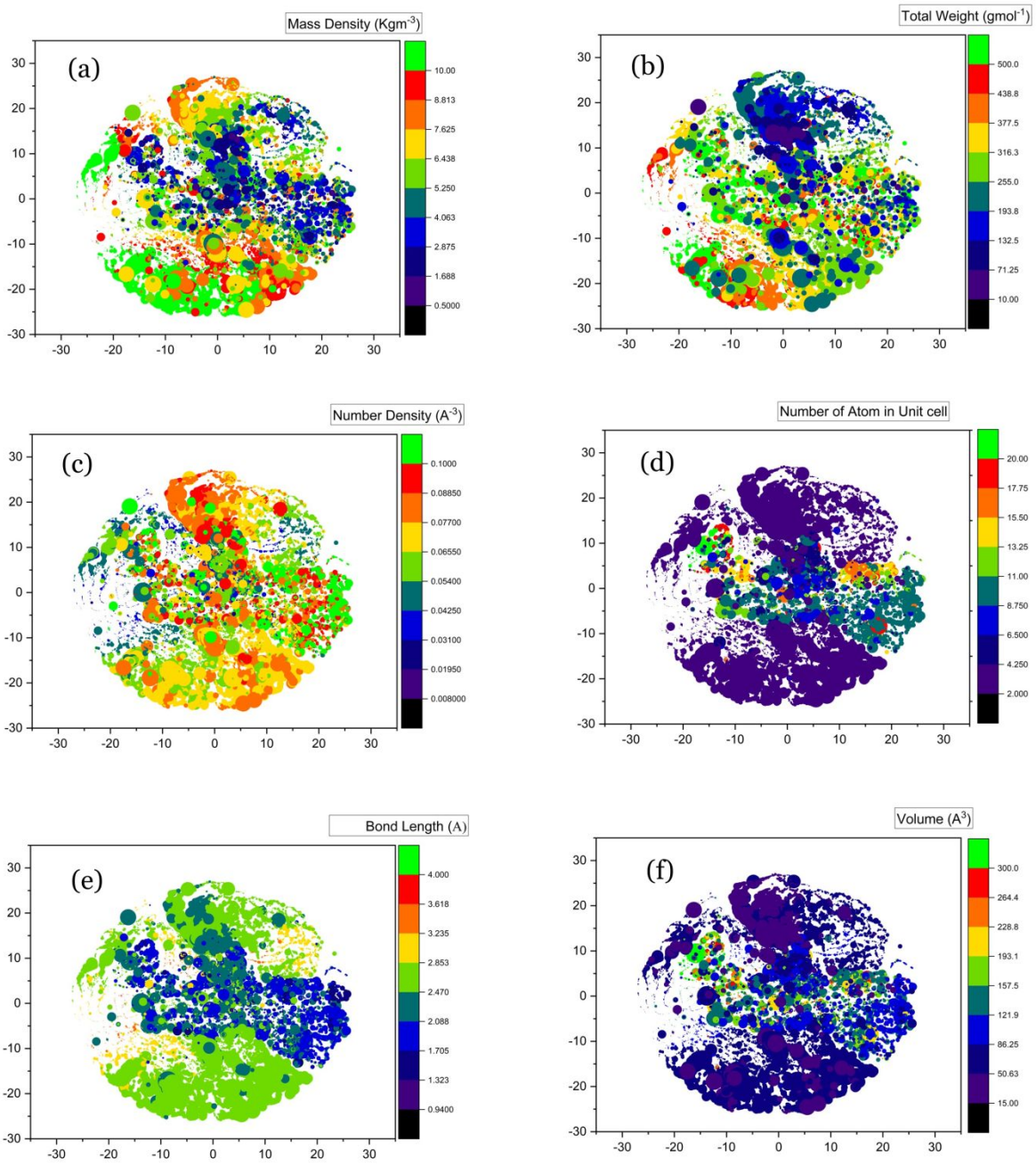

Figure 7: t-SNE plot with perplexity of 50 showing analysis and insight into the different magnitude of LTC (size of circle) among all 22,899 predicted structures. (a) mass density, (b) total weight, (c) number density, (d) number of atoms in primitive cell, (e) bond length, and (f) volume distribution.

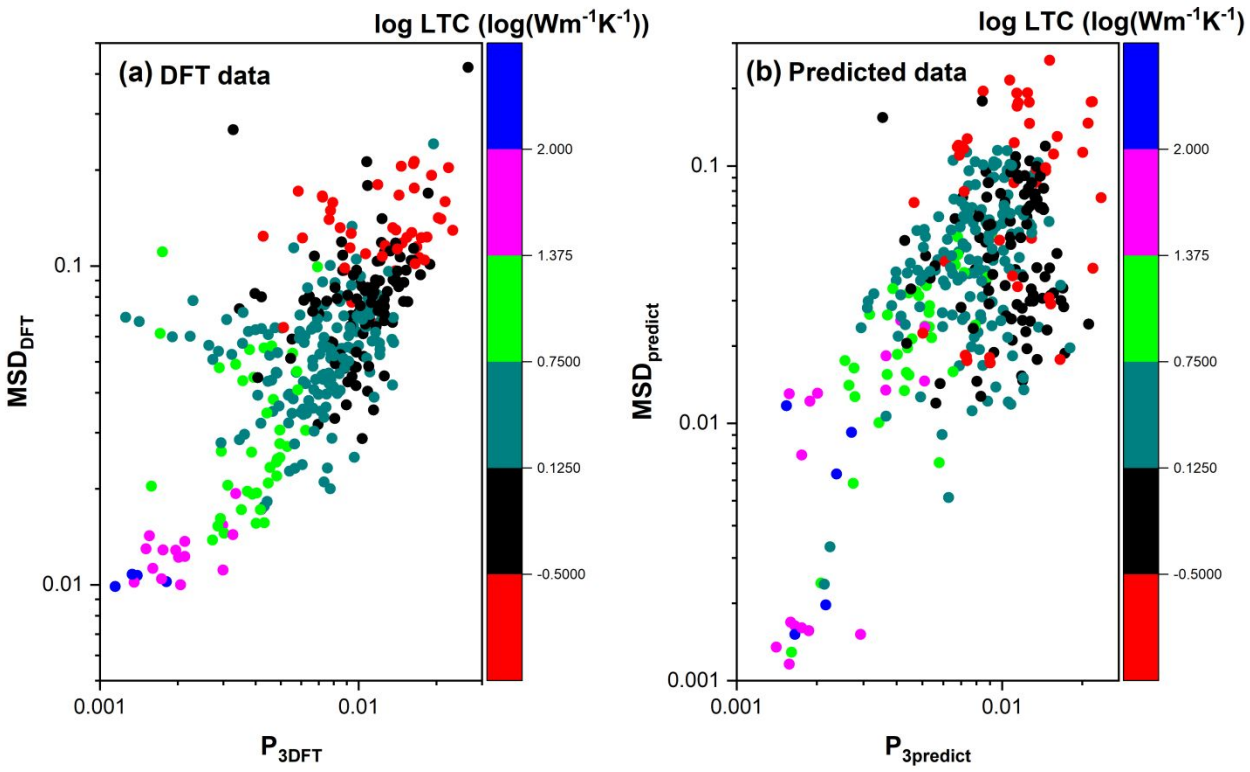

Figure 8: Three-phonon scattering phase space (P_3 parameter) versus thermal mean squared displacement (MSD) of the 359 low lattice thermal conductivity (LTC) structures by (a) DFT calculations and (b) ALIGNN model predictions. The color bar represents the logarithmic value of LTC. Both panels clearly show the same trend that the P_3 parameter and MSD are negatively correlated with LTC, and thus the large P_3 parameter and large MSD are good material descriptors for quick screening materials with ultralow LTC.